Translational Oncology 25 (2022) 101524

Contents lists available at ScienceDirect

Translational Oncology

journal homepage: www.elsevier.com/locate/tranon

Original Research

Pyroptosis-related lncRNA pairs to estimate the molecular features and prognostic outcomes of pancreatic ductal adenocarcinoma

Si-Yuan Lu [a,b,c,d,†], Jie Hua [a,b,c,d,†], Jiang Liu [a,b,c,d,†], Miao-Yan Wei [a,b,c,d], Chen Liang [a,b,c,d], Qing-Cai Meng [a,b,c,d], Bo Zhang [a,b,c,d], Xian-Jun Yu [a,b,c,d], Wei Wang [a,b,c,d,*], Jin Xu [a,b,c,d,**]

[a] Department of Pancreatic Surgery, Fudan University Shanghai Cancer Center, Shanghai, PR. China
[b] Department of Oncology, Shanghai Medical College, Fudan University, Shanghai, PR. China
[c] Shanghai Pancreatic Cancer Institute, Shanghai, PR. China
[d] Pancreatic Cancer Institute, Fudan University, Shanghai, PR. China

ARTICLE INFO

Keywords:
Pancreatic dual adenocarcinoma
Pyroptosis
Bioinformatics analysis
Immune infiltration
Drug sensitivity

ABSTRACT

Pyroptosis is a form of programmed cell death associated with inflammatory alterations. However, the intrinsic mechanisms and underlying correlation of pyroptosis-related lncRNAs (PRLs) in pancreatic ductal adenocarcinoma (PDAC) remain unclear. The objective of the current research was to identify pyroptosis-related lncRNAs and a prognostic model to predict the prognosis of patients. We extracted pyroptosis-related lncRNAs to construct a risk model and validated them at Fudan University Shanghai Cancer Center. Crosstalk between lncRNA SNHG10 and GSDMD was found to regulate pyroptosis levels. A new algorithm was used to establish a 0 or 1 PRL pair matrix and prognostic model. Six pyroptosis-related lncRNA pairs were identified and utilized to construct a risk model. The low-risk groups exhibited better prognoses than the high-risk groups. The area under the curve (AUC) indicated extremely high accuracy, reaching 0.810 at 1 year, 0.850 at 2 years, and 0.850 at 3 years in the training set. Patients with different risk scores exhibited distinct metabolic, inflammatory, and immune microenvironments as well as tumor mutation landscapes. Additionally, 9 commonly used chemotherapeutic drugs exhibited different sensitivities between the high- and low-risk groups. To conclude, we propose that pyroptosis exhibits a close correlation with PDAC. Our risk model based on PRL pairs may be beneficial for the accurate estimation of prognostic outcomes, the immune microenvironment, and drug sensitivity, bringing therapeutic hope for patients with PDAC.

Introduction

Pancreatic cancer is one of the most aggressive and malignant tumors, with a five-year survival rate of less than 9% [1]. As the most common pathological type of pancreatic cancer, pancreatic ductal adenocarcinoma (PDAC) often attracts attention but lacks satisfactory therapeutic results [2]. A cold microenvironment makes tumors insensitive to chemotherapy and immunotherapy, and this may be the most important cause of unsatisfactory treatment outcomes [2,3]. Therefore, it is urgent to find new molecular targets and therapeutic strategies for PDAC. Pyroptosis, a form of programmed cell death that leads to cell lysis, has been implicated in inflammation and the gasdermin family [4]. Current evidence has elucidated that pyroptosis may affect innate and adaptive immunity and can also promote chimeric antigen receptor T-cell therapy (CAR-T) and immune checkpoint inhibitor (ICI) therapy [5]. Notably, pyroptosis-related research may bring new hope to patients with PDAC.

Previous studies on pyroptosis mainly focused on executive pyroptosis proteins such as the gasdermin family (GSDMs) [6] and inflammation-associated lyases such as caspase1/3/4/5 [7]. For example, caspase3/gasdermin E-mediated pyroptosis was demonstrated to inhibit the malignant proliferation and migration of triple-negative breast cancer cells [8]. However, the intrinsic mechanism of lncRNA-mediated pyroptosis regulation remains complex and

* Corresponding author at: Shanghai Pancreatic Cancer Institute, No. 270 Dong'An Road, Shanghai 200032, PR. China.
** Corresponding author at: Department of Pancreatic Surgery, Fudan University Shanghai Cancer Center, No. 270 Dong'An Road, Shanghai 200032, PR. China.
E-mail addresses: wangwei@fudanpci.org (W. Wang), xujin@fudanpci.org (J. Xu).
† These authors contributed equally to this work.

https://doi.org/10.1016/j.tranon.2022.101524
Received 18 May 2022; Received in revised form 9 August 2022; Accepted 24 August 2022

enigmatic. Zhang *et al*. eliminated that the lncRNA MEG3 regulated the pyroptosis of endothelial cells by interacting with NLRP3 [9]. Recent studies also indicated that lncRNAs may modulate the occurrence and progression of malignant tumors through ceRNA networks. For example, the lncRNA TP53TG1 was found to influence the proliferation and migration of PDAC cells by binding to miR-96 [10]. Zhong *et al*. demonstrated that the lncRNA Sox2ot served as a ceRNA to regulate invasion, metastasis and stemness through the Sox2ot/miR200/Sox2 axis [11]. Nevertheless, the innate mechanism by which lncRNAs regulate the occurrence and development of PDAC through pyroptosis has not been explored. The identification of pyroptosis-related lncRNAs (PRLs) and associated prognostic markers may lead to new breakthroughs in the underlying molecular mechanisms and clinical treatment of PDAC.

In the present research, comprehensive bioinformatics analysis was performed to identify PRLs and construct a pyroptosis-related lncRNA model (PRLM) that can accurately distinguish patients with different prognoses, metabolic reprogramming, immune and inflammatory microenvironments, mutation landscapes, and drug sensitivities. The pattern flowchart in Figure S1 shows our research design.

Materials and methods

Acquisition of transcriptome data, clinical data and mutation data

The transcriptome data and clinical data of 182 pancreatic cancer patients were downloaded from the UCSC Zena database. The clinical data, including sex, race, age, total tumor stage, T stage, N stage of the American Joint Committee on Cancer (AJCC), and alcohol history, were included for prognostic analysis. A total of 142 patients with PDAC remained after eliminating patients with other neoplasms and with incomplete clinical information. The mutation data of these PADC samples were extracted from the UCSC Zena database in varscan2. Genomic subtype information was extracted from a previously published study [12].

Detection of pyroptosis

We identified pyroptosis by detecting critical proteins, including csapase1, caspase4, caspase5, GSDMD, and IL18. Quantitative real-time polymerase chain reaction (qRT–PCR) was used to calculate the relative expression of these molecules.

Identification and pairing of PRLs

Pyroptosis-related genes (PRGs) were extracted from GeneCards (https://www.genecards.org/) and published studies. The mRNAs and lncRNAs were annotated according to the annotation file in the UCSC Zena database. PRLs were identified by correlation analysis between PRGs and lncRNAs, with a P value $\langle$ 0.001 and a correlation coefficient $\rangle$ 0.5 considered significant. LncRNAs were paired cyclically and unrepetitively, and a "0″ or "1″ matrix was established according to the relative expression of lncRNA A or lncRNA B in the lncRNA pairs (lncRNA A- lncRNA B). A lncRNA pair was defined as 1 if the expression of lncRNA A was higher than that of lncRNA B; otherwise, it was defined as 0. The lncRNA pair was thought to be invalid and was excluded when its number of 0 or 1 exceeded 80% or less than 20% of the total number.

Construction of a PRL pair model (PRLM) to assess the prognosis of PDAC

Multiple machine learning algorithms were utilized to screen valid lncRNA pairs for model construction. Univariate analysis was used to identify lncRNA pairs with prognostic significance, followed by Lasso regression analysis to eliminate overfitting and complete coefficient compression and a random forest algorithm to improve prediction accuracy. The intersection of the Lasso regression and random forest results was incorporated into the multivariate Cox regression model to eliminate multicollinearity and construct the final predictive model. The risk score formula: risk score = $expr_{pair1}$ * $coff_{pair1}$+ $expr_{pair2}$ * $coff_{pair2}$+… … $expr_{pairn}$ * $coff_{pairn}$. The R packages "survminer" and "survival" were utilized to draw survival curves. Additionally, we identified 4 prognostic pyroptosis inhibitors and 15 prognostic pyroptosis promotors from the PRGs and calculated the pyroptosis-related index (PRI) using the "GSVA" R package. To validate the clinical value of our PRLM, we extracted 80 paraffin-embedded specimens from the previously mentioned FUSCC cohort, and qRT–PCR was performed to confirm its application value. We used delta CT to define the relative expression of lncRNAs and translated it into a "0" or "1" matrix according the aforementioned method.

Evaluation of the enriched pathways and alterations in critical metabolism patterns according to the PRLM

To elucidate the alterations in the critical biological processes and functional pathways in PDAC, we identified the differentially expressed genes between different PRLM groups. In addition, we obtained metabolism-related gene sets from KEGG database and annotated them with the "GSVA" package. The variation in metabolic rewriting between different PRLM groups was accurately analyzed.

Estimation of the mutational landscape based on the PRLM

To assess the correlation between the mutational landscape and PRLM scores, we analyzed and evaluated various perspectives. The "maftools" R package was used to process and depict the mutation data. The differences in tumor mutation burden and mutation form between different PRLM risk groups were compared, with a P value $<$ 0.05 considered significant.

Significance of the PRLM in immune infiltration and the microenvironment

Various published immune assessment algorithms, including ssGSEA, XCELL, TIMER, EPIC, QUANTISEQ, CIBERSORT and MCP-counter, were used to evaluate immune infiltration. We compare the differences in immune infiltration between different PRLM risk groups. Additionally, the correlation between immune cell infiltration and the PRLM score was analyzed by Spearman's correlation analysis. Furthermore, a heatmap was generated to exhibit the variations in critical checkpoints between the various PRLM groups.

Drug sensitivity analysis based on the PRLM

The R package "pRRophetic" was utilized to predict the drug IC50 in the different PRLM risk groups. This algorithm can calculate the IC50 of chemotherapeutic drugs according to the gene expression matrix information and then accurately predict drug sensitivity. We used the Wilcoxon test to compare the differences in drug IC50 values between the various risk groups. Spearman analysis was performed to calculate the correlation between drug IC50 values and PRLM scores.

Cell culture and qRT–PCR

Paraffin-embedded specimens from 80 FUSCC patients were utilized to identify the expression levels of core lncRNAs. The patients had undergone standard pancreatic cancer resection and had complete follow-up information. Additionally, one human normal pancreatic cell line (H6C7) and six human pancreatic cancer cell lines (PANC-1, Mia-PaCa2, SW 1990, ASPC-1, CFPAC-1, and BxPC-3) were chosen to verify the expression levels of core lncRNAs. The expression of candidate lncRNAs was determined using an ABI 7900HT Real-Time PCR system (Applied Biosystems, Foster City, MA, USA). The primers in the research are summarized in Supplementary Table 1.

Flow cytometry

Flow cytometry experiments were utilized to detect the apoptosis rate of various groups. The PE Annexin V Apoptosis Detection Kit (Beyotime Biotechnology, Shang Hai, China, cat: 559763) was used for staining, and a FACSCalibur flow cytometer was used for counting.

Transwell migration assay

To detect the migration ability, PANC-1 cells (5×10^4 cells) were cultured in the upper chamber to determine their migration capacity. We counted the number of migrating cells in a random area, and an average of 5 fields per chamber was assessed.

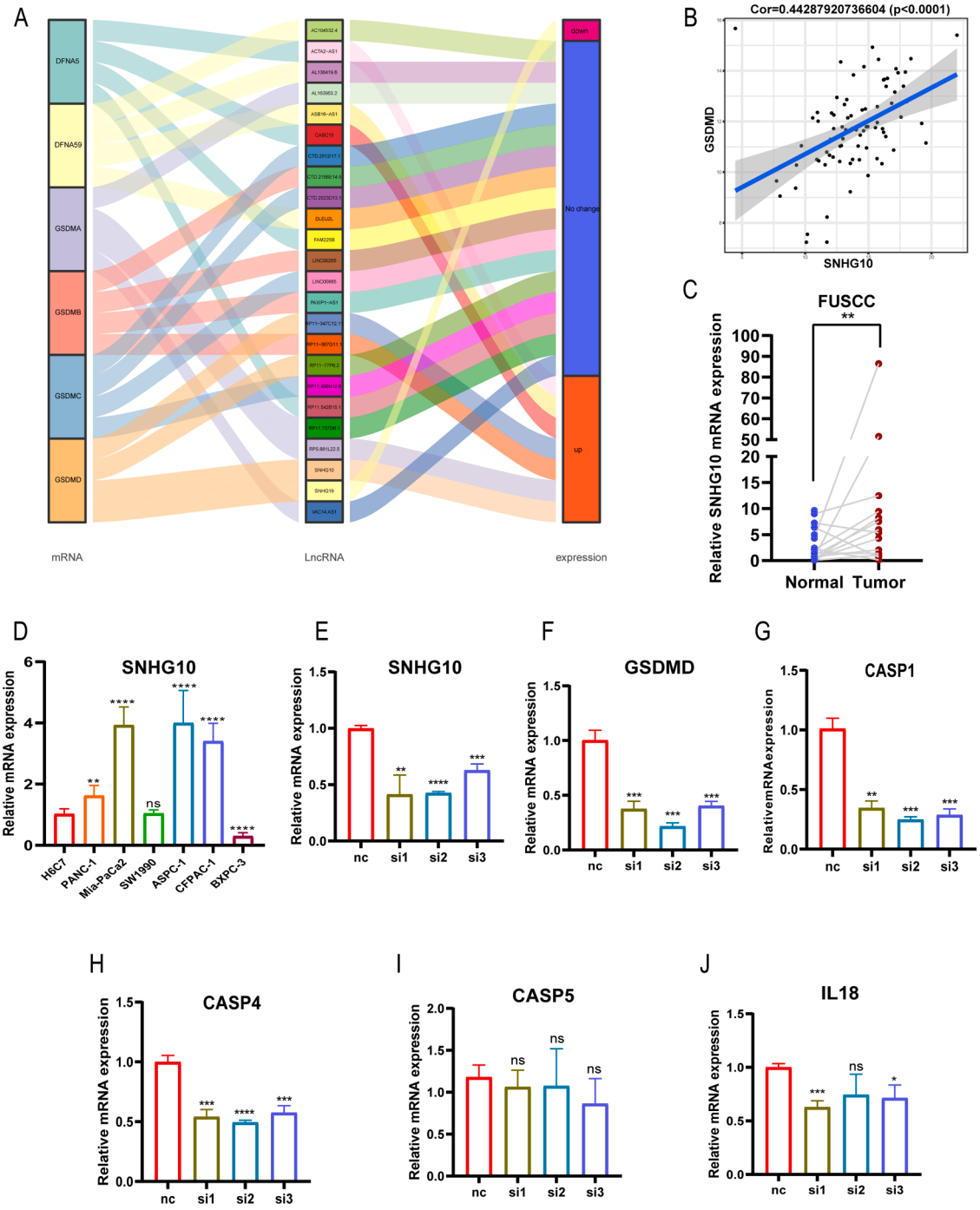

Fig. 1. Identification of potential PRLs and experimental validation of the regulatory effects of SNHG10 on pyroptosis. (A) The correlation between core PRGs, corresponding lncRNAs and expression conditions. (B) SNHG10 was positively correlated with the expression of GSDMD. (C) SNHG10 exhibited elevated expression in tumor samples. (D) SNHG10 expression was upregulated in multiple pancreatic cancer cell lines. (E) The expression of SNHG10 in PANC-1 was knocked down. (F) The expression level of GSDMD was downregulated after SNHG10 knockdown. (G-I) The expression level alterations of CASP1, CASP4, CASP5, and IL18. $^*P < 0.05$, $^{**}P < 0.01$, $^{***}P < 0.001$, $^{****}P < 0.0001$.

EdU assay

To detect the proliferation capacity, PANC-1 cells (3×10^4 cells) were cultured in 96-well plates with 5 replicate wells. The specific experiment was performed as described in our previous study [13].

CCK-8 assays

PANC-1 cells (1500 cells) were cultured in 96-well plates with 4 replicate wells to detect cell viability and proliferation ability. Cells were incubated with CCK-8 (Gaithersburg, MD, USA) for two hours, and a microplate reader (Tecan F50, Switzerland) was used to measure the absorbance at 450 nm.

Soft agar colony formation assays

For the soft agar colony formation assays, Panc-1 cells (3000/well) were cultured in DMEM with 15% FBS and 0.2% agarose, and then the complex was layered on DMEM with 15% FBS and 0.3% agarose in 6-well plates with 3 duplicated holes. These cells were fixed and stained with 4% paraformaldehyde and 0.5% crystal violet.

Animal studies

We obtained five-week-old nude mice from Shanghai Laboratory Animal Center. Each mouse was inoculated with 2 × 106 Panc-1 cells. We divided these mice into two groups: a group treated with si-control (5 nmol) (used for animals, RuiBo, Shanghai, China) and a group treated with si-SNHG10 (5 nmol) (used for animals, RuiBo, Shanghai, China) every 3 days for 4 weeks. We measured the tumor size every week, and the tumors were excised and weighed after four weeks. The Ethics Committee of Fudan University approved our experimental protocol (FUSCC-IACUC-2,022,166).

Results

Identification of PRLs using coexpression analysis and experimental validation

A total of 113 PRGs and 14,831 lncRNAs were identified and integrated into a coexpression matrix. In total, 2639 PRLs were significantly coexpressed with PRGs based on the inclusion criteria, with a P value $<$ 0.001 and correlation coefficient $>$ 0.5. Additionally, 364 PRLs were found to exhibit prognostic value and to be related to the overall survival of PDAC. Some lncRNAs were remarkably positively correlated with critical pyroptosis regulators, including DFNA5, DFNA59, GSDMA, GSDMB, GSDMC, and GSDMD (Fig. 1A). GSDMD is a typical pyroptosis-inducing molecule that is targeted by autoprocessed caspases and was found to be inhibited by disulfiram [14,15]. In the results of the correlation analysis, GSDMD was found to be positively correlated with SNHG10 ($r = 0.58$, $P < 0.001$), which may promote the proliferation, migration, and progression of various malignancies [16,17]. In addition, we also identified pyroptosis-associated microRNAs and circRNAs, explored their relationship with pyroptosis regulators and clarified their expression levels in pancreatic cancer (Figure S2).

To further validate the potential function of SNHG10 in PDAC, paraffin-embedded specimens from 80 FUSCC patients, which contained 16 pairs of pancreatic cancer and adjacent samples, were analyzed in the current study. SNHG10 was found to be positively correlated with the expression of GSDMD ($r = 0.442$, $P<0.0001$) (Fig. 1B) and exhibited elevated expression in tumor samples (Fig. 1C). The cytological results indicated that the expression of SNHG10 was upregulated in multiple pancreatic cancer cell lines, including PANC-1, Mia-PaCa2, ASPC-1, and CFPAC-1 (Fig. 1D). Furthermore, we knocked down the expression of SNHG10 in PANC-1 cells through small interfering RNA and detected fluctuations in pyroptosis levels (Fig. 1E). The expression level of GSDMD was significantly downregulated after SNHG10 was knocked down (Fig. 1F). Additionally, we detected the expression of some core molecules of pyroptosis, including CASP1, CASP4, CASP5 and IL18, which mostly showed a downward trend (Fig. 1G-1I), demonstrating the decrease in intracellular pyroptosis and the capacity of SNHG10 to regulate pyroptosis in PDAC. We further explored the effects of SNHG10 on proliferation, apoptosis and metastasis with functional experiments. The apoptosis ratio of PANC-1 cells was not remarkably influenced by gene silencing and only exhibited a small increase (Figure S3). The proliferation capacity of SNHG10 knockdown cells was decreased compared to that of the control groups (Fig. 2A-2B). The CCK-8 experiment further proved this result (Fig. 2C). The colony formation in soft agar results indicated that the control group showed stronger colony ability than the SNHG10 si group (Fig. 2D-2E). Additionally, SNHG10-silenced cells exhibited lower migration ability in the Transwell migration experiment (Fig. 2F-2G). To explore the potential role of SNHG10 in vivo tumorigenicity in pancreatic cancer, we established pancreatic xenograft tumors and administered different treatments to different groups of mice (Fig. 2H). The results indicated that the tumors of mice in the SNHG10 si group were significantly smaller than those of the control group (Fig. 2I), and there were also significant differences in tumor weight (Fig. 2J), which further suggested that SNHG10 played a promoting role in pancreatic cancer tumorigenesis.

The PRLM risk signature can accurately identify the prognosis of patients with PDAC

A total of 364 PRLs were screened as mentioned and reintegrated into a “0” or “1” matrix containing 21,886 lncRNA pairs. In total, 270 lncRNA pairs associated with overall survival were retained after univariate Cox regression analysis. After Lasso regression analysis (Figure S4A-S4B) and random forest analysis to reduce overfitting and improve accuracy, 7 lncRNA pairs remained in the intersection (Figure S4C). Six lncRNA pairs were finally included in the PRLM after multivariate Cox regression analysis to avoid collinearity (Figure S4D). The risk score plot exhibited the risk distribution and survival status (Fig. 3A). A Kaplan–Meier curve was generated to evaluate the predictive effectiveness (Fig. 3B), and patients with different risk scores were divided into two risk groups according to the medium cutoff value. The low-risk group exhibited significantly better prognoses than the high-risk group. A ROC curve was drawn to verify the sensitivity and accuracy of the PRLM (Fig. 3C). The AUC values for 1, 2, and 3 years were 0.81, 0.85, and 0.85, respectively. To estimate the clinical value of the PRLM, we performed univariate and multivariate Cox regression analyses on the PRLM combined with some important clinical parameters. Multivariate analysis indicated that PRLM had superior predictive capacity and was an independent prognostic factor for PDAC (Fig. 3D-3E). To further verify its practicality and reliability, an external cohort from FUSCC was used. Significant differences in survival were exhibited between the various groups (Fig. 3F), and the AUCs at 1 (0.87) and 2 years (0.85) illustrated the potential clinical value of the PRLM (Fig. 3G). We performed meticulous subtype classification based on the final screened lncRNA pairs, and the ConsensusCluster algorithm was used to complete this classification process. According to the cumulative distribution function (CDF) value and CDF area change, $k = 2$ exhibited the best unsupervised clustering competence (Figure S5A). The principal component analysis (PCA) plot further validated the independence of the clustering subtype (Figure S5B). Interestingly, certain differences were determined between our unsupervised clustering and PRLM, which may be complementary to our PRLM-related grouping (Figure S5C). The survival curve indicated that subtype 1 exhibited a longer average survival time than subtype 2 (Figure S5D).

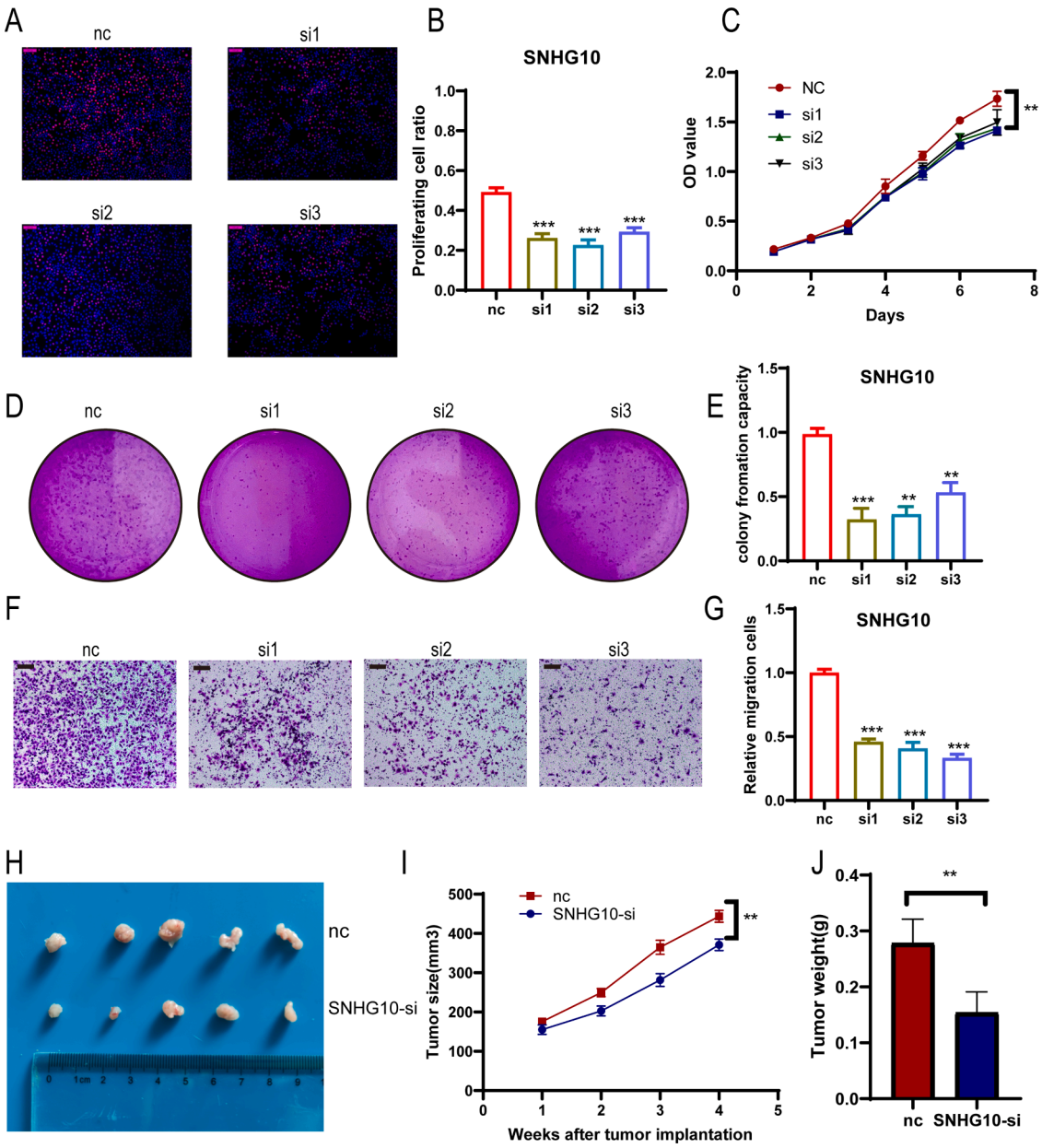

Fig. 2. Influence of SNHG10 on the proliferation, migration and tumorigenesis in PDAC. (A, B) EDU experiments demonstrate the proliferation ability of different PANC-1 treatment groups. (C) CCK-8 assay to detect the proliferation ability of PANC-1 cells transferred with SNHG10 siRNA. (D, E) The soft agar colony formation experiment to detect the colony formation ability of different PANC-1 treatment groups. (F, G) The influence of SNHG10 on the migration of PANC-1 cells. (H) The image of tumors excised from different treatment groups. (I) the tumor size of different treatment groups. (J) the tumor weight of different treatment groups. Scale bars, 100 μm. *$P < 0.05$, **$P < 0.01$, ***$P < 0.001$, ****$P < 0.0001$.

Comprehensive analysis of enriched pathways and metabolic reprogramming

We identified 1757 differentially expressed genes between different PRLM groups and included them in the functional annotation analysis. Gene Ontology (GO) analysis indicated that these genes were mainly involved in some metabolism-related physiological processes, including "regulation of lipid metabolic process", "negative regulation of protein phosphorylation", "regulation of lipase activity", and "canonical glycolysis" (Fig. 4A). KEGG analysis also suggested that these genes were related to some metabolism-related pathways, such as "Proteoglycans in cancer", "Central carbon metabolism in cancer", "Regulation of lipolysis in adipocytes", and "Carbohydrate digestion and absorption" (Fig. 4B). Furthermore, we explored the alterations in metabolic reprogramming between the high- and low-PRLM subgroups. A total of 7347 metabolism-related pathways from the KEGG database were annotated and analyzed, such as lipid modification, ion transport, carbohydrate process, and steroid biosynthetic process. Metabolic pathway analysis indicated that a total of 24 metabolism-related processes were differentially expressed between the high- and low-PRLM groups, including 15 upregulated metabolic pathways in the PRLM high-risk group, such as N glycan biosynthesis and glycolysis and gluconeogenesis, and nine downregulated metabolic pathways, such as fatty acid metabolism and glycerolipid metabolism (Fig. 4C). We further divided these metabolic pathways into nucleic acid metabolism, lipid metabolism, glucose metabolism, protein metabolism and other metabolic pathways. Coexpression analysis demonstrated that these pathways closely interacted, which further indicated alterations in metabolic reprogramming in PDAC (Fig. 4D).

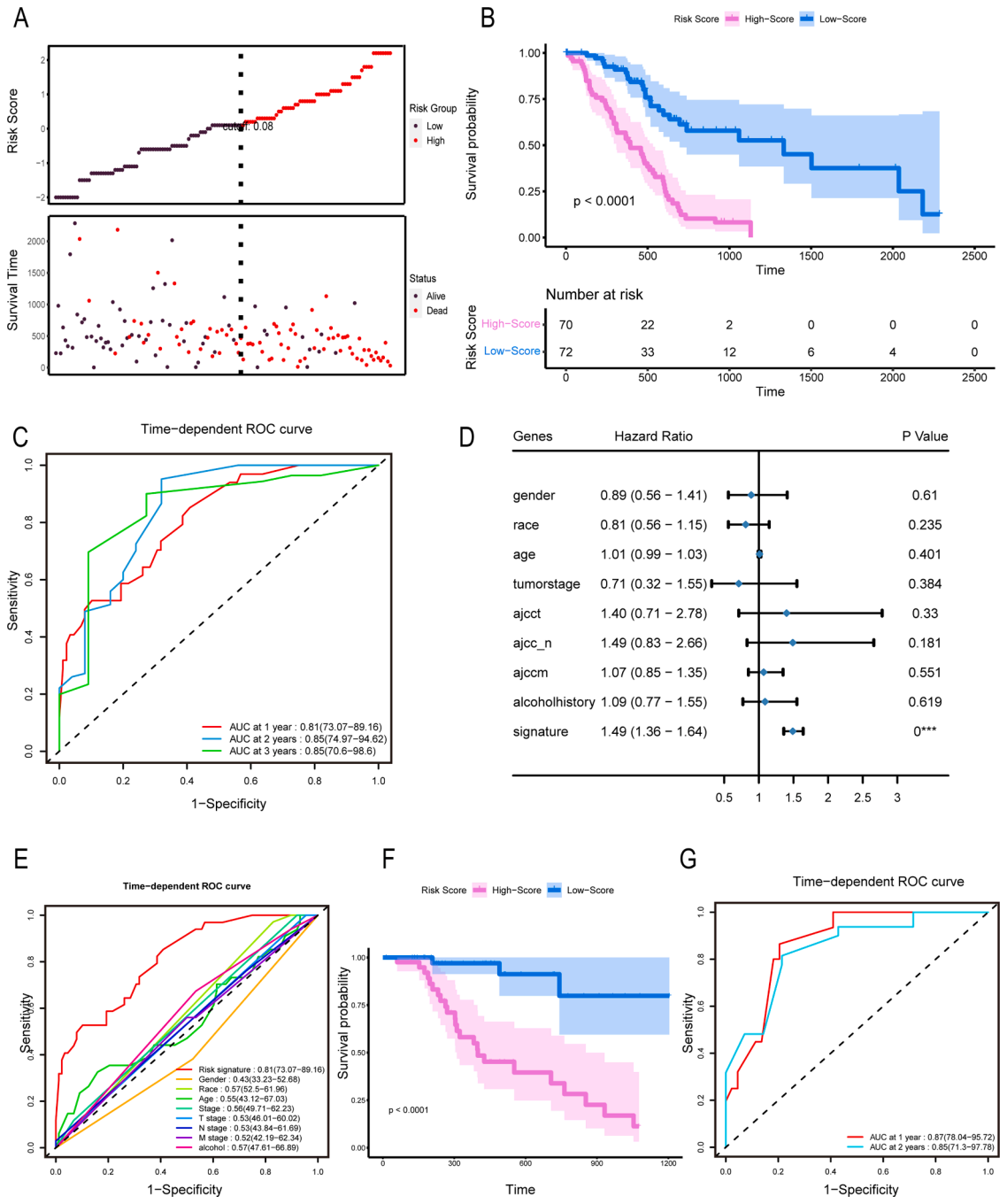

Fig. 3. Construction of a PRL pair model (PRLM) to assess the prognosis of PDAC. (A) The risk score plot shows the risk distribution and survival status. (B) A Kaplan–Meier curve was used to evaluate the predictive effectiveness. (C). A ROC curve was used to verify the sensitivity and accuracy of the PRLM. (D) Forest plot of multivariate Cox regression analysis based on the risk signature and clinical parameters. (E) A ROC curve was used to estimate the effectiveness of the PRLM and some clinical parameters. (F) A Kaplan–Meier curve was used to validate the PRLM in FUSCC. (G) A ROC curve was used to validate the PRLM in FUSCC.

Identification of differences in immune infiltration and the inflammatory microenvironment between the high- and low-PRLM groups

We comprehensively analyzed and compared the differences between PRLM and previously published molecular subtypes in PDAC and found that our PRLM was an independent classification (Fig. 5A-5C). Seven different immune infiltration algorithms, ssGSEA, XCELL, TIMER, EPIC, QUANTISEQ, CIBERSORT and MCP-counter, were used to annotate and analyze the immune microenvironment of PDAC. Coexpression exploration was performed between the PRLM score and various immune cells, and the results indicated that most of the tumor-resistant immune cells, such as active CD8+ T cells, Th1 cells, and dendritic cells, were negatively related to the PRLM score (Fig. 5D). To further explore the feasibility of the PRLM in immune checkpoint therapy, we analyzed the expression of various immune checkpoints in different PRLM groups. Most immune checkpoints, including CTLA4, PDCD1, and LAG3, exhibited higher expression activity in the low-PRLM group, demonstrating great potential for PRLM grouping in immune checkpoint therapy (Fig. 5E). Differences in some critical immune microenvironment-related scores were also compared. The low-PRLM group exhibited upregulated immune scores, stromal scores, microenvironment scores, and ESTIMATE scores, demonstrating stronger immune infiltration activity (Fig. 5F). We also explored the differences in the inflammatory microenvironment between various groups.

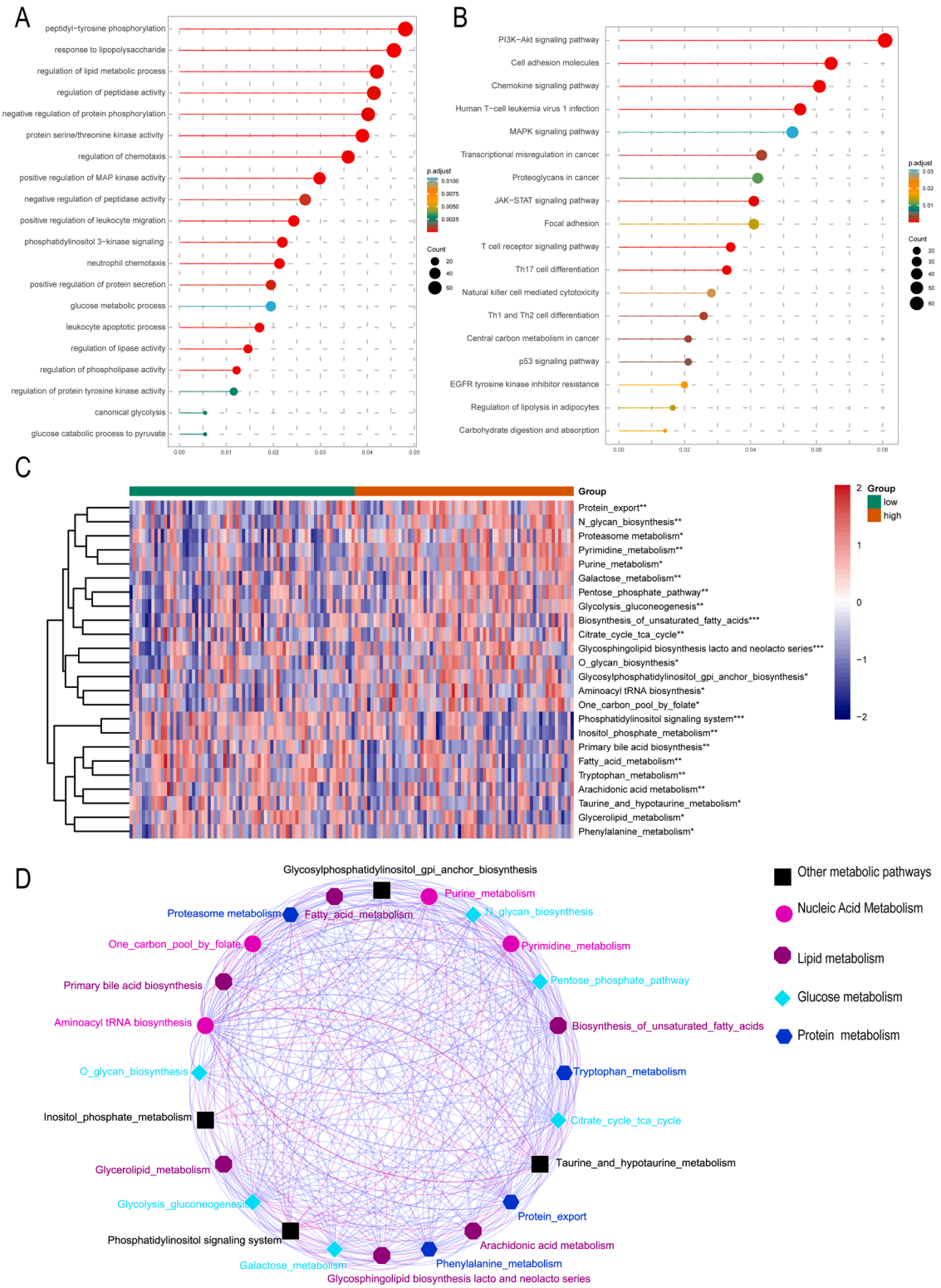

Fig. 4. Comprehensive analysis of enriched pathways and metabolic reprogramming. (A) GO analysis based on differentially expressed genes. (B) KEGG analysis based on differentially expressed genes. (C) The differentially expressed metabolic pathways between the high- and low-PRLM groups. (D) Coexpression analysis of metabolic pathways. *$P < 0.05$, **$P < 0.01$, ***$P < 0.001$, ****$P < 0.0001$.

Inflammatory factors exhibited significantly upregulated expression activity in the low-PRLM group (Figure S6).

Comparison of the PRLM with the PRI in PDAC

The expression profiles of PRGs in different PRLM groups were explored, and 19 differentially expressed pyroptosis regulators were identified, including 15 pyroptosis promotors and 4 pyroptosis inhibitors (Fig. 6A, S7A). We further calculated the PRI of every sample according to these pyroptosis regulators and compared it with the PRLM. The samples were divided into two groups based on the PRI (Fig. 6B). The PRI exhibited identical fluctuation trends as the PRLM,

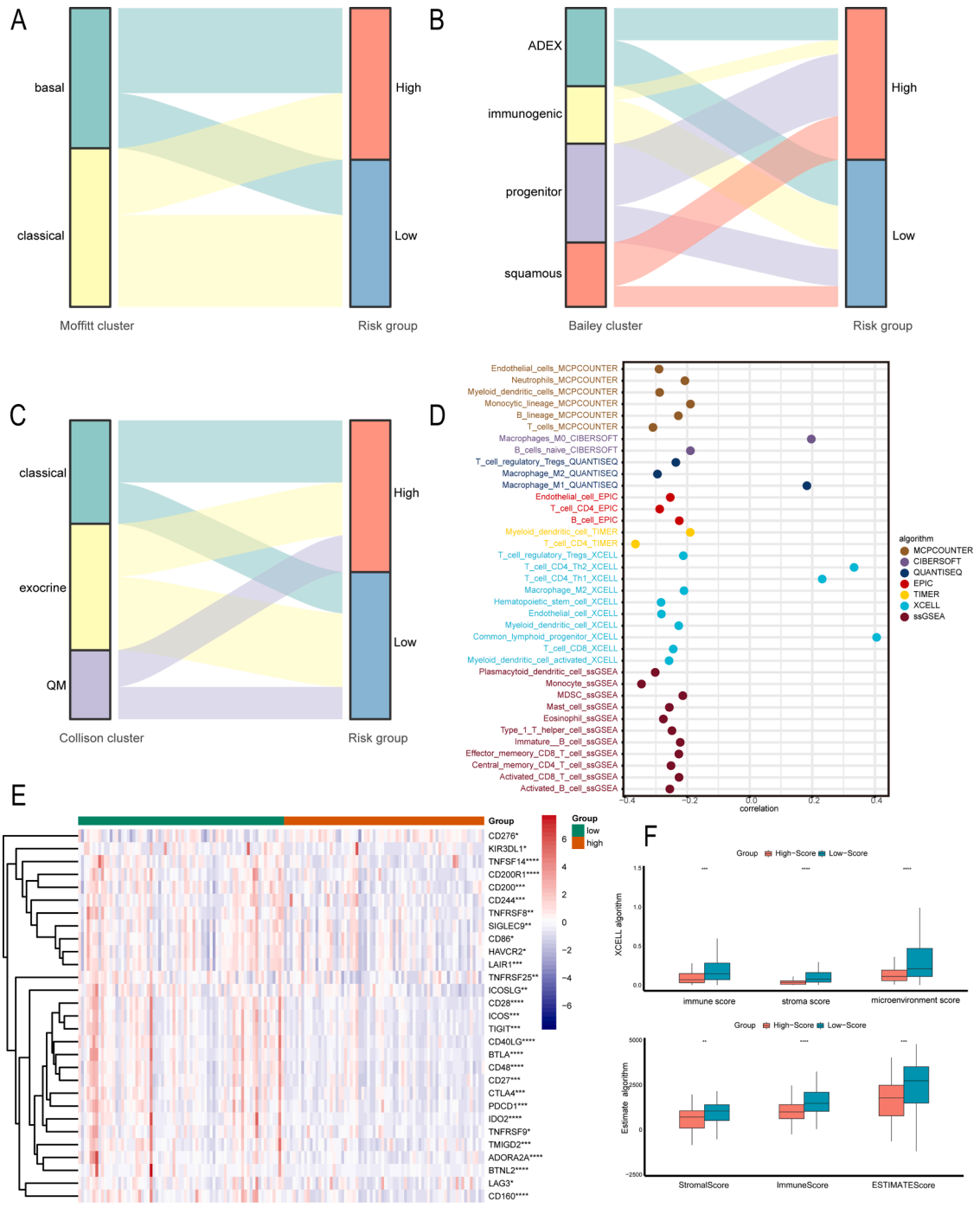

Fig. 5. Identification of differences in immune infiltration and the inflammatory microenvironment between the high- and low-PRLM groups. (A-C) The differences between the PRLM and previously published molecular subtypes in PDAC. (D) Coexpression exploration between the PRLM score and various immune cells. (E) The expression of various immune checkpoints in different PRLM groups. (F) Differences in the inflammatory microenvironment between the high- and low-PRLM groups. $^{*}P < 0.05$, $^{**}P < 0.01$, $^{***}P < 0.001$, $^{****}P < 0.0001$.

and it increased as the PRLM score increased. Similarly, the PRI-high group exhibited higher PRLM scores, further validating the rationality of our PRLM (Fig. 6C). A pyroptosis-related risk signature based on these differentially expressed pyroptosis regulators was established and compared to the PRLM. The survival curve exhibited good predictive performance (Figure S7B), but the AUC was remarkably lower than that of our PRLM, further demonstrating the superiority of our PRLM (Figure S7C).

Comparison of the mutational landscape in different PRLM risk groups

The mutational landscape in different PRLM risk groups was compared. The high-PRLM group exhibited remarkably higher TMB scores (Fig. 7A). Mutation type comparisons demonstrated that the high-PRLM group exhibited a higher mutation rate in some mutant forms, such as in frame deletions, missense mutations, nonsense mutations, and silent mutations (Fig. 7B). The waterfall plot indicated that KRAS, TP53, COKN2D, and SMAD4 exhibited the highest mutation frequencies in all groups (Fig. 7C, 7D). Comutation analysis indicated that KRAS/TP53

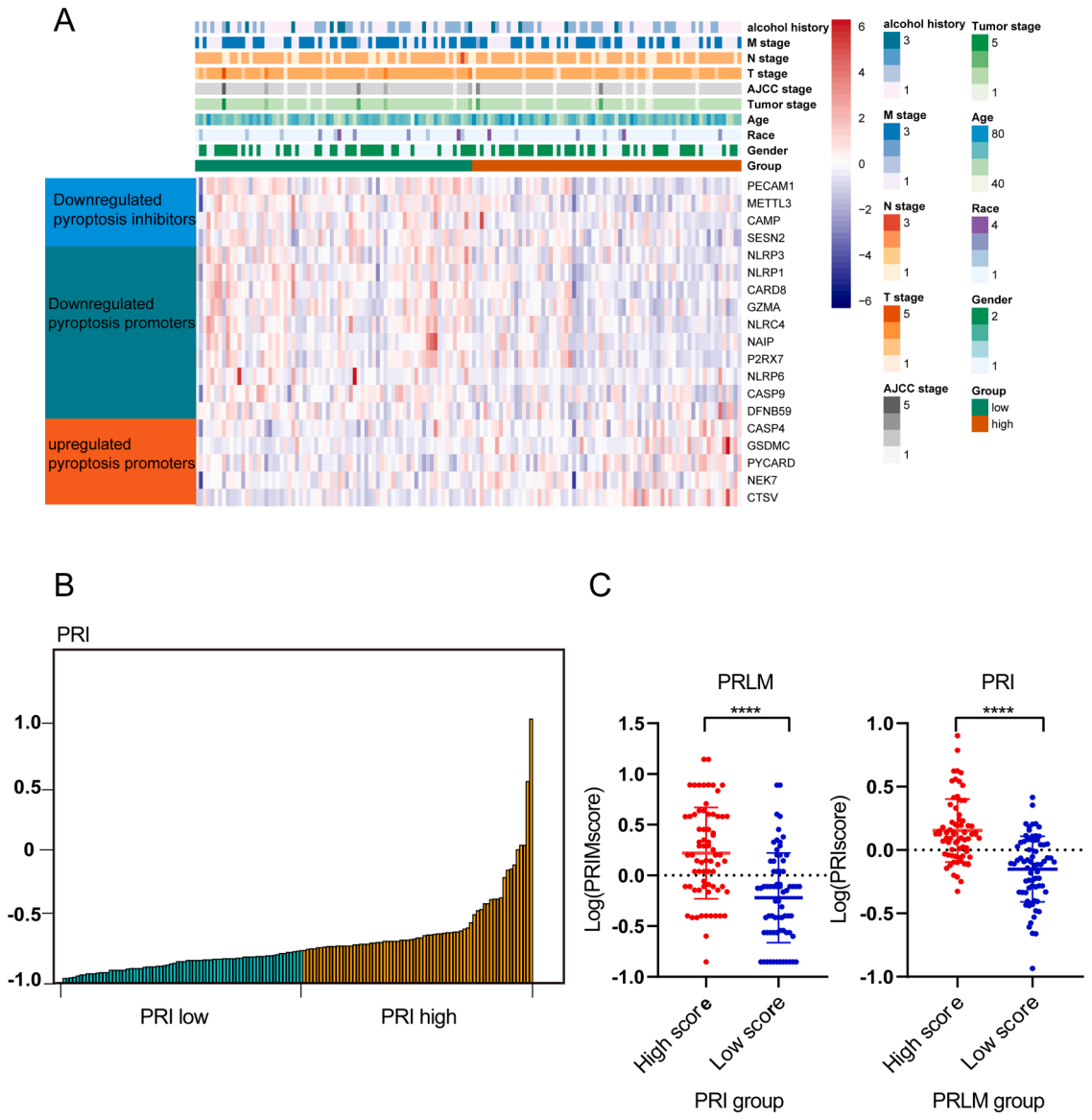

Fig. 6. Comparison of PRLM with PRI in PDAC. (A) The expression pattern of pyroptosis regulators. (B) The samples were divided into two groups based on the PRI. (C) Comparison between PRI and PRLM. *$P < 0.05$, **$P < 0.01$, ***$P < 0.001$, ****$P < 0.0001$.

and CDKN2A/TP53 may be comutation pairs in the low-PRLM group (Fig. 7E). In addition, the high-PRLM group exhibited more comutation pairs, including KRAS/TP53, CDKN2A/TP53, MUC16/SMAD4, and TTN/PCDH15 (Fig. 7F).

Predictive value of the PRLM risk signature for chemotherapeutic sensitivity

Drug sensitivity analysis was utilized to eluminated the application value of the PRLM in drug effectiveness prediction. The IC50 values of 27 commonly used chemotherapeutic drugs were calculated, and we investigated their correlation with the PRLM score. The IC50 values of most drugs were negatively correlated with the PRLM score, and a few were positively correlated (Fig. 8A). We further compared the change in drug IC50 values between the various PRLM groups and found that 9 drugs exhibited significant differences, including paclitaxel, erlotinib and other commonly used drugs for PDAC (Fig. 8B, 8C), indicating that the PRLM not only has a guiding role in chemotherapeutic drug usage in PDAC but may also have predictive significance for other anticancer drugs.

DISCUSSION

Pyroptosis is a programmed cell death process closely related to internal inflammation and the immune response [18], and it has been proven to be a double-edged sword in the occurrence and development of various tumors [6]. Dysregulation of GSDMD may perturb pyroptosis and influence cell phase progression, leading to an imbalance in cell proliferation in gastric cancer [19]. More interestingly, pyroptosis may modulate the immune microenvironment and anticancer therapy through inflammatory cytokines from cancer cells [5], bringing new prospects to the therapy of solid tumors such as PDAC that are prone to chemotherapy resistance [20]. However, the innate mechanism of pyroptosis in cancer prognosis and the microenvironment remains unclear, especially in the lncRNA field. Tan *et al.* found that the lncRNA HOTTIP may function as a tumor promotor by increasing AKT2 expression and inducing inflammatory pyroptosis [21]. Additional crosstalk between pyroptosis and lncRNAs was identified in liver cancer. Chen *et al.* demonstrated the regulatory role of the lncRNA SNHG7, which may interact with the pyroptosis modulator NLRP3 [22]. Therefore, determining PRLs and exploring the interaction between PRLs and

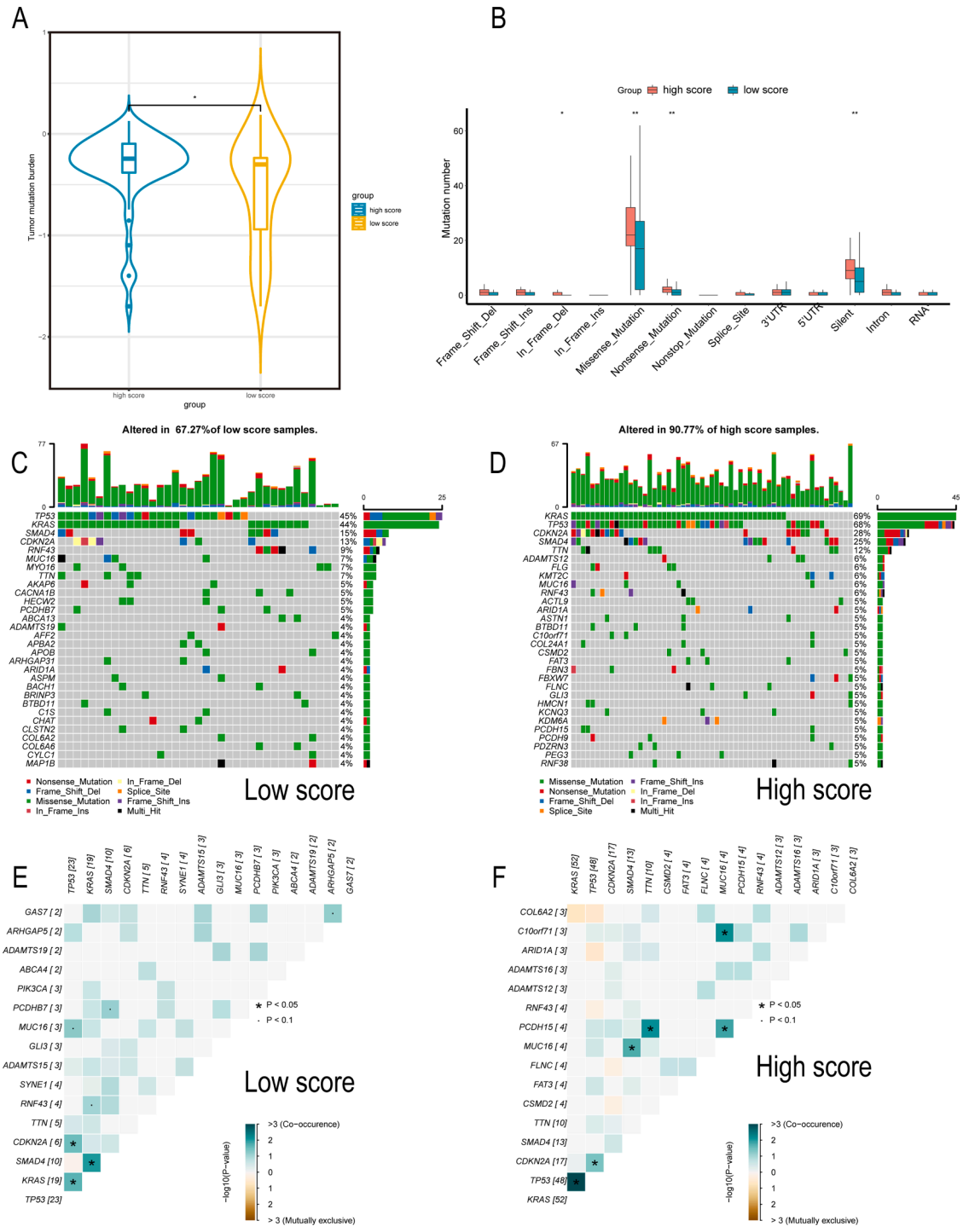

Fig. 7. Comparison of the mutational landscape in different PRLM risk groups. (A) Comparison of the TMB score between the high-risk and low-risk groups. (B) Comparison of the mutation forms between the high-risk and low-risk groups. (C, D) The waterfall plot depicts the mutated genes of patients in different risk groups. (E, F) The coexpression plots show the coexpressed genes in the high- and low-risk groups. *$P < 0.05$, **$P < 0.01$, ***$P < 0.001$, ****$P < 0.0001$.

PRGs may be a forward-looking approach and lead to further findings. In our current research, multiple PRL and PRG pairs were identified, and a PRLM was constructed to estimate the metabolic reprogramming, immune and inflammatory microenvironments, mutation landscape, and drug sensitivity in PDAC. Additionally, the GSDMD-related lncRNA SNHG10 was identified, and biological experiments were conducted to validate its potential role in pyroptosis.

SNHG10 serves as a tumor promoter in various malignancies, including osteosarcoma [23], non-small cell lung cancer [24], and hepatocellular carcinoma [25]. In our research, we found that SNHG10 was elevated not only in multiple pancreatic cancer cell lines but also in pancreatic cancer tissues. Furthermore, SNHG10 may also promote the proliferation and migration capacity of pancreatic cancer cells, illustrating its oncogenic potential. We also demonstrated that SNHG10 was positively coexpressed with the pyroptotic regulator GSDMD, and it could affect the pyroptotic status through caspase1, IL18, etc. Therefore, we hypothesized that SNHG10 may affect the biological behavior, occurrence and development of PDAC by affecting pyroptosis, and the

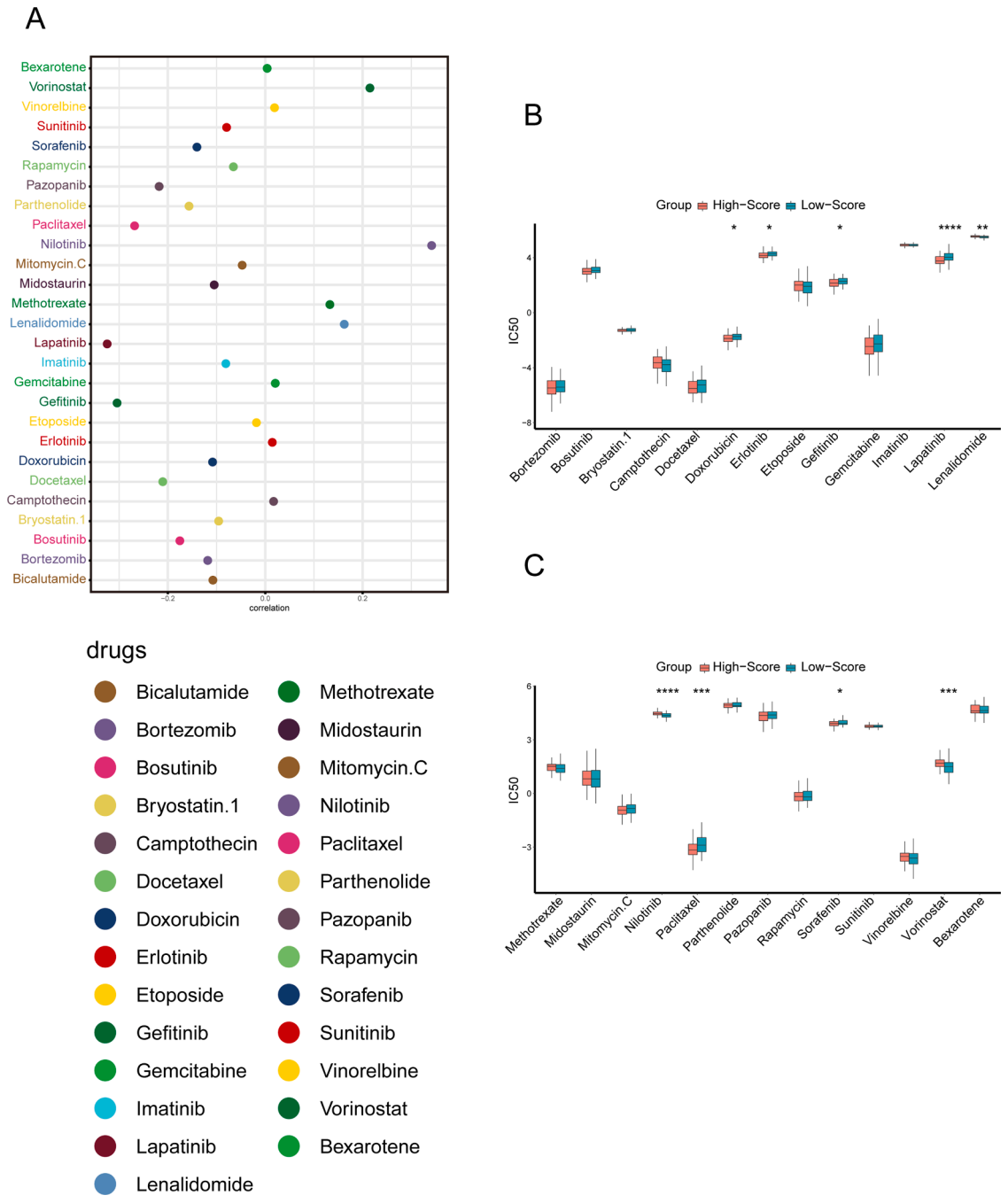

Fig. 8. Predictive value of the PRLM risk signature for chemotherapeutic sensitivity. (A) The correlation between the PRLM score and IC50 values of 27 drugs. (B, C). The difference in drug IC50 values between the high- and low-PRLM groups. *$P < 0.05$, **$P < 0.01$, ***$P < 0.001$, ****$P < 0.0001$.

concrete underlying mechanism needs to be further explored by additional molecular biology and animal experiments.

Previous major discoveries about pyroptosis and tumors mainly focused on intrinsic molecular mechanisms and inflammatory alterations [5]. Our research was the first to explore the potential effect of pyroptosis on metabolic reprogramming in PDAC. The basic metabolic patterns, including nucleic acid metabolism, lipid metabolism, glucose metabolism, and protein metabolism, were altered in the different PRLM groups, indicating that metabolic reprogramming may be involved in pyroptosis-related carcinogenic mechanisms. The combined analysis of pyroptosis and metabolism may bring new breakthroughs to mechanistic research in PDAC.

Recent studies have illustrated the crosstalk between malignancies and the immune microenvironment [26]. Currently, impressive immunotherapy methods have achieved profound success in a small number of cancer patients, but the efficacy in most patients remains unsatisfactory [27]. Pyroptosis-related cancer research may be beneficial to anticancer immunotherapy. Notably, we highlighted that immune infiltration was significantly negatively correlated with the PRLM score, especially some anticancer immune cells, such as active CD8+ T cells and Th1 cells. Additionally, some typical immune checkpoints and cytokines, such as PDCD1 and IL6, exhibited upregulated trends in the low-PRLM group, indicating that drugs targeting these molecules may be effective treatment measures for these patients.

Our research has some undeniable strengths. First, there have been many studies on the prognostic prediction of pyroptosis-related genes or lncRNAs in the past [28,29]. Our study first proposed the establishment of a prognostic model based on PRL pairs, filling the gap in this area.

Second, the previous studies constructed algorithms mostly based on gene expression. Notably, due to differences in platforms and the subjectivity of different researchers, applying their model may lead to substantial deviation and yield biased results. Our research used a 0 or 1 matrix as a measure of relative expression, avoiding platform bias and enhancing applicability. Our PRLM achieved optimal predictive competence (AUC> 0.85). Third, we not only identified SNHG10 as a key molecule regulating pyroptosis in PDAC but also validated our PRLM in our FUSCC cohort.

Our research also has some limitations. On the one hand, our screening criteria for PRLs were consistent with those of published research [28,29] based on coexpression analysis and the magnitude of the correlation coefficient, not based on biological experiments. On the other hand, the number of samples in our FUSCC cohort was relatively small, and our PRLM needs to be further validated in a larger dataset. In conclusion, our current research first identified PRLs and constructed a PRLM in PDAC, realizing optimal predictive capacity for the prognosis of patients. Additionally, we comprehensively analyzed the ability of the PRLM to discriminate PDAC metabolic reprogramming, immune microenvironments, mutational landscapes, and drug sensitivities. We expect to find new approaches for PDAC treatment based on these research directions and apply our PRLM to clinical treatment.

Authors' contributions

SYL, JH, MYW, CL, QCM, and JL analysed the data. JX and WW revised the manuscript. WW and XJY proposed the idea of the article and revised the manuscript. All authors read and approved the final manuscript.

Funding

This study was jointly supported by the National Natural Science Foundation of China (82072698; 82103551, U21A20374), Shanghai Municipal Science and Technology Major Project (21JC1401500), Scientific Innovation Project of Shanghai Education Committee (2019–01–07–00–07-E00057), Clinical Research Plan of Shanghai Hospital Development Center (SHDC2020CR1006A), and Xuhui District Artificial Intelligence Medical Hospital Cooperation Project (2021–011).

Conflict of Interest

The authors declare that they have no competing interests.

Acknowledgments

Not applicable.

Supplementary materials

Supplementary material associated with this article can be found, in the online version, at doi:10.1016/j.tranon.2022.101524.

References

[1] R.L. Siegel, K.D. Miller, A. Jemal, Cancer statistics, 2020, CA Cancer J. Clin. 70 (1) (2020) 7–30.
[2] W. Park, A. Chawla, O'reilly EM, Pancreatic Cancer: a Review, JAMA 326 (9) (2021) 851–862.
[3] C. Dolladille, S. Ederhy, M. Sassier, et al., Immune Checkpoint Inhibitor Rechallenge After Immune-Related Adverse Events in Patients With Cancer, JAMA Oncol. 6 (6) (2020) 865–871.
[4] Y. Wang, T.D. Kanneganti, From pyroptosis, apoptosis and necroptosis to PANoptosis: a mechanistic compendium of programmed cell death pathways, Comput Struct Biotechnol. J 19 (2021) 4641–4657.
[5] S.K. Hsu, C.Y. Li, I.L. Lin, et al., Inflammation-related pyroptosis, a novel programmed cell death pathway, and its crosstalk with immune therapy in cancer treatment, Theranostics 11 (18) (2021) 8813–8835.
[6] X. Xia, X. Wang, Z. Cheng, et al., The role of pyroptosis in cancer: pro-cancer or pro-"host"? Cell Death. Dis. 10 (9) (2019) 650.
[7] Y. Fang, S. Tian, Y. Pan, et al., Pyroptosis: a new frontier in cancer, Biomed. Pharmacother. 121 (2020), 109595.
[8] H. An, J.S. Heo, P. Kim, et al., Tetraarsenic hexoxide enhances generation of mitochondrial ROS to promote pyroptosis by inducing the activation of caspase-3/GSDME in triple-negative breast cancer cells, Cell Death. Dis. 12 (2) (2021) 159.
[9] Y. Zhang, X. Liu, X. Bai, et al., Melatonin prevents endothelial cell pyroptosis via regulation of long noncoding RNA MEG3/miR-223/NLRP3 axis, J. Pineal Res. 64 (2) (2018).
[10] Y. Zhang, H. Yang, Y. Du, et al., Long noncoding RNA TP53TG1 promotes pancreatic ductal adenocarcinoma development by acting as a molecular sponge of microRNA-96, Cancer Sci. 110 (9) (2019) 2760–2772.
[11] Z. Li, P. Jiang, J. Li, et al., Tumor-derived exosomal lnc-Sox2ot promotes EMT and stemness by acting as a ceRNA in pancreatic ductal adenocarcinoma, Oncogene 37 (28) (2018) 3822–3838.
[12] Integrated Genomic Characterization of Pancreatic Ductal Adenocarcinoma, Cancer Cell 32 (2) (2017) 185–203. .e113.
[13] S. Lu, J. Hua, J. Liu, et al., Comprehensive analysis of the prognosis and immune infiltration landscape of RNA methylation-related subtypes in pancreatic cancer, BMC Cancer 22 (1) (2022) 804.
[14] J.J. Hu, X. Liu, S. Xia, et al., FDA-approved disulfiram inhibits pyroptosis by blocking gasdermin D pore formation, Nat. Immunol. 21 (7) (2020) 736–745.
[15] K. Wang, Q. Sun, X. Zhong, et al., Structural mechanism for GSDMD targeting by autoprocessed caspases in pyroptosis, Cell 180 (5) (2020) 941–955. .e920.
[16] Y. Zhang, H. Guo, H. Zhang, SNHG10/DDX54/PBX3 Feedback loop contributes to gastric cancer cell growth, Dig. Dis. Sci. 66 (6) (2021) 1875–1884.
[17] X. Yuan, T. Yang, Y. Xu, et al., SNHG10 promotes cell proliferation and migration in gastric cancer by targeting miR-495-3p/CTNNB1 Axis, Dig. Dis. Sci. 66 (8) (2021) 2627–2636.
[18] Y.Y. Wang, X.L. Liu, R. Zhao, Induction of pyroptosis and its implications in cancer management, Front. Oncol. 9 (2019) 971.
[19] L. Gopinathan, S.L. Tan, V.C. Padmakumar, V. Coppola, L. Tessarollo, P. Kaldis, Loss of Cdk2 and cyclin A2 impairs cell proliferation and tumorigenesis, Cancer Res. 74 (14) (2014) 3870–3879.
[20] M.P. Kim, G.E. Gallick, Gemcitabine resistance in pancreatic cancer: picking the key players, Clin. Cancer Res. 14 (5) (2008) 1284–1285.
[21] C. Tan, W. Liu, Z.H. Zheng, X.G. Wan, LncRNA HOTTIP inhibits cell pyroptosis by targeting miR-148a-3p/AKT2 axis in ovarian cancer, Cell Biol. Int. 45 (7) (2021) 1487–1497.
[22] Z. Chen, M. He, J. Chen, C. Li, Q. Zhang, Long non-coding RNA SNHG7 inhibits NLRP3-dependent pyroptosis by targeting the miR-34a/SIRT1 axis in liver cancer, Oncol. Lett. 20 (1) (2020) 893–901.
[23] S. Zhu, Y. Liu, X. Wang, J. Wang, G. Xi, lncRNA SNHG10 promotes the proliferation and invasion of osteosarcoma via Wnt/β-Catenin Signaling, Mol. Ther. Nucleic Acids 22 (2020) 957–970.
[24] Z. Zhang, L. Nong, M.L. Chen, et al., Long noncoding RNA SNHG10 sponges miR-543 to upregulate tumor suppressive SIRT1 in nonsmall cell lung cancer, Cancer Biother. Radiopharm. 35 (10) (2020) 771–775.
[25] T. Lan, K. Yuan, X. Yan, et al., LncRNA SNHG10 facilitates hepatocarcinogenesis and metastasis by modulating its homolog SCARNA13 via a positive feedback loop, Cancer Res. 79 (13) (2019) 3220–3234.
[26] S.K. Dougan, The pancreatic cancer microenvironment, Cancer journal 23 (6) (2017) 321–325 *(Sudbury, Mass.)*.
[27] Z. Zhang, Y. Zhang, J. Lieberman, Lighting a fire: can we harness pyroptosis to ignite antitumor immunity? Cancer Immunol. Res. 9 (1) (2021) 2–7.
[28] W. Lv, Y. Tan, C. Zhao, et al., Identification of pyroptosis-related lncRNAs for constructing a prognostic model and their correlation with immune infiltration in breast cancer, J. Cell. Mol. Med. 25 (22) (2021) 10403–10417.
[29] X. Chen, H. Chen, H. Yao, et al., Turning up the heat on non-immunoreactive tumors: pyroptosis influences the tumor immune microenvironment in bladder cancer, Oncogene 40 (45) (2021) 6381–6393.